Trabecular Microfracture Precedes Cortical Shell Failure in the Rat Caudal Vertebra Under Cyclic Overloading

S. R. Kummari · A. J. Davis · L. A. Vega ·
N. Ahn · E. H. Cassinelli · C. J. Hernandez

Abstract Microscopic tissue damage has been observed in otherwise healthy cancellous bone in humans and is believed to contribute to bone fragility and increased fracture risk. Animal models to study microscopic tissue damage and repair in cancellous bone would be useful, but it is currently not clear how loads applied to a whole animal bone are related to the amount and type of resulting microdamage in cancellous bone. In the current study we determine the relationship between applied cyclic compressive overloading and the resulting amount of microdamage in isolated rat tail vertebrae, a bone that has been used previously for in vivo loading experiments. Rat caudal vertebrae (C7–C9, $n = 22$) were potted in bone cement and subjected to cyclic compressive loading from 0 to 260 N. Loading was terminated in the secondary and tertiary phases of the creep-fatigue curve using custom data-monitoring software. In cancellous bone, trabecular microfracture was the primary form of microdamage observed with few microcracks. Trabecular microfracture prevalence increased with the amount of cyclic loading and occurred in nine out of 10 specimens loaded into the tertiary phase. Only small amounts of microdamage were observed in the cortical shell of the vertebrae, demonstrating that, under axial cyclic loading, damage occurs primarily in regions of cancellous bone before overt fracture of the bone (macroscopic cracks in the cortical shell). These experiments in isolated rat tail vertebrae suggest that it may be possible to use an animal model to study the generation and repair of microscopic tissue damage in cancellous bone.

Microdamage in the form of microscopic cracks and diffuse damage has been observed in vivo in both human cortical bone [1–4] and cancellous bone [5–7]. In cancellous bone, microdamage may also take the form of trabecular microfractures (complete fracture of trabeculae) [8–12]. Microdamage is associated with reductions in the elastic modulus and strength of bone [13] and is believed to influence clinical fracture. Microscopic tissue damage has been implicated as a contributor to clinical fractures, particularly those that are not caused by a single loading event, such as stress fractures and vertebral fractures [14, 15]. Once microdamage is formed in bone, it remains until it is removed by repair processes such as bone remodeling or fracture healing (i.e., callus). As a result, the amount of microdamage in a bone is influenced by both microdamage formation and microdamage repair.

The rat ulna loading model [16] is the most popular method used to examine the repair of microdamage in cortical bone [17, 18]. In vivo animal models for studying microdamage in cancellous bone are rare and have so far been limited to studies with implants [19–21]. Only one of these approaches has been used to examine microscopic tissue damage [21]. A disadvantage of techniques using implants is that application of the implant requires damaging the cortical shell and surrounding periosteum,

S. R. Kummari · A. J. Davis · L. A. Vega · C. J. Hernandez (✉)
Musculoskeletal Mechanics and Materials Laboratory,
Department of Mechanical and Aerospace Engineering,
Case Western Reserve University, Glennan 615A,
10900 Euclid Ave., Cleveland, OH 44106, USA
e-mail: christopher.hernandez@case.edu

N. Ahn · E. H. Cassinelli
Department of Orthopedic Surgery,
Case Western Reserve University, Cleveland, OH, USA

potentially influencing the type of microdamage formed and altering any repair processes [20].

The rat tail loading model [22] in which pins are placed in two tail vertebrae (C7 and C9 typically) and used to apply axial loads to the intermediary vertebra, is an attractive approach for applying microdamage to a region of cancellous bone because it does not involve placing an implant in the bone of interest. However, because rat tail vertebrae have thick cortical shells it is not clear that their axial loading will result in microdamage in cancellous bone. Additionally, it is not clear what type of microdamage (microscopic cracks, diffuse damage, trabecular microfracture) can be generated in the rat caudal vertebra under axial loading and where that damage is located (metaphyseal cancellous bone, cortical shell, etc.).

The long-term goal of this project is to understand how microdamage is repaired in cancellous bone. Toward that goal, the current study evaluates the relationship between applied cyclic loading and the amount, type, and location of microdamage in rat tail vertebrae.

Materials and Methods

Caudal vertebrae (C7–C9) from adult female Sprague-Dawley rats (375–425 g) were included in this study. A total of 22 caudal vertebrae from eight animals were examined. All animal use was approved by the Case Western Reserve University Institutional Animal Care and Use Committee. Bones were dissected free of soft tissues. To prevent the possibility of damaging the underlying bone tissue, any soft tissue that could not be removed through gentle dissection was left intact (typically small clumps of disc or periosteum). The distal and proximal ends of each bone were potted within flat depressions in cylindrical stainless steel platens using bone cement (Technovit 3040 kit; EBSciences, East Granby, CT). Specimen alignment in the center of the plates was assured using custom fixtures. Bone cement covered no more than 0.8 mm of each end of the vertebrae. Drops of saline solution were applied to the vertebral body, while the bone cement cured to maintain hydration. Once the cement dried, a thin strip of saline-soaked gauze was wrapped around the bone to maintain hydration. The platens were then mounted in a material testing device (EnduraTech ELF 3400; Bose, Eden Prairie, MN) (Fig. 1).

Mechanical Testing

Once mounted in the testing device, a sinusoidal cyclic load ranging from 0 to 260 N was applied at 2 Hz in a materials testing device (Bose EnduraTech ELF 3400). The peak force of 260 N was chosen based on preliminary data
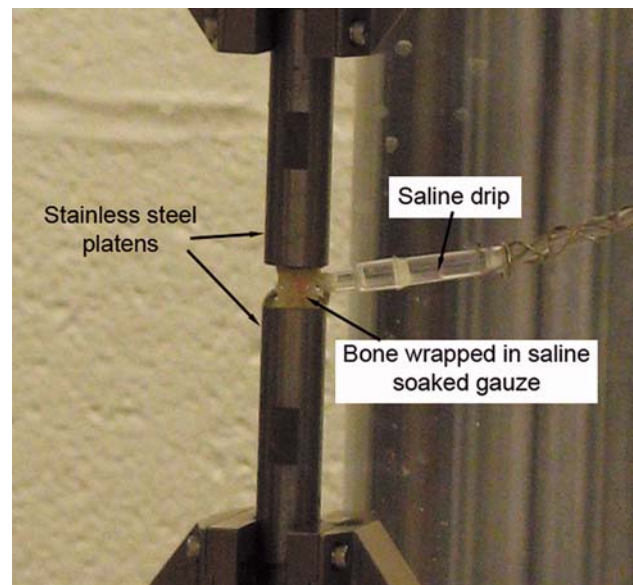

Fig. 1 Rat caudal vertebrae were aligned within stainless-steel platens and potted with bone cement
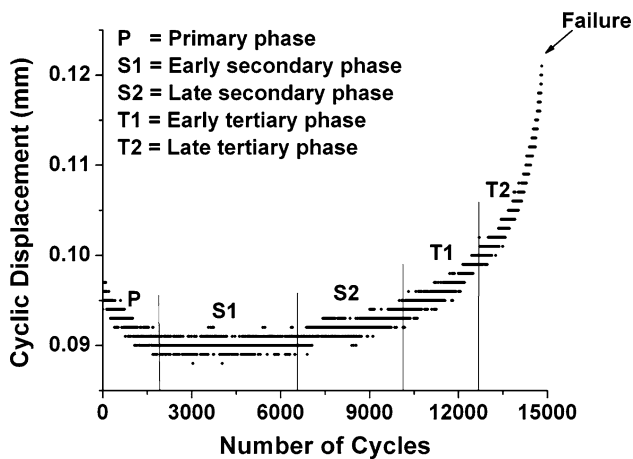
which implied that cyclic loading would continue beyond 2 h to provide a moderate number of cycles before failure. A saline drip was applied throughout testing to maintain hydration.

Alterations in peak displacement during cyclic loading can be divided into two components: creep displacement and cyclic displacement (Fig. 2). The displacement at minimum load (relative to the initial position) was defined as creep displacement, and the difference between the maximum and the minimum displacement in each cycle was defined as cyclic displacement [18]. Alterations in creep displacement and cyclic displacement over time were divided into three phases: primary, secondary, and tertiary (Figs. 2, 3). The primary phase includes a sudden increase in creep displacement and a slight decrease in cyclic displacement. In the secondary phase, creep displacement increases at a steady rate, while cyclic displacement changes very little. Both creep displacement and cyclic displacement increase rapidly in the tertiary phase.

Cyclic loading was applied until a prescribed alteration in the rate of change of cyclic displacement. This made it possible to capture the state of the system after damage had occurred but before failure (Fig. 3). Using this approach it was possible to stop fatigue loading within the tertiary phase prior to failure. A custom program written in the Bose dynamic testing programming language (WinTest v3.0) was used to evaluate the rate of change in cyclic displacement during the test. Cyclic loading was divided into blocks of 100 cycles. At the end of each block, average cyclic displacement for the block was calculated and compared with that of the previous block of 100 cycles. If
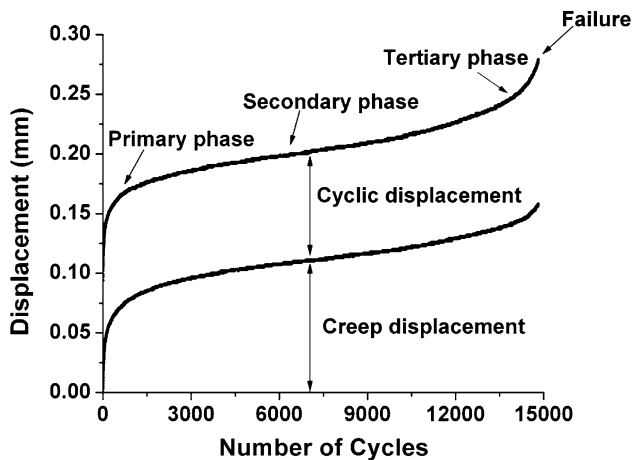
Fig. 2 Variation of maximum and minimum displacements during cyclic loading are shown. Maximum displacement can be divided into two components, creep displacement and cyclic displacement [18]. Different phases of the cyclic loading curve are indicated

Fig. 3 Changes in cyclic displacement during loading are shown. The five study groups are classified based on rate of change of cyclic displacement

Table 1 Study groups classified by their positions on the creep–fatigue curve

Groups	Rate of change of cyclic displacement (μ/cycle)	Sample size
Unloaded (U)	–	3
Early secondary (S1)	0–0.5	4
Late secondary (S2)	0.5–1.0	5
Early tertiary (T1)	1.0–1.6	6
Late tertiary (T2)	>1.6	4

through inspection of the cyclic displacement vs. number of cycles curve). Three specimens that were not loaded at all were used as a control group. Two additional specimens that had failed during our preliminary studies were included as positive controls. Sample sizes for these five study groups are listed in Table 1, and their relative positions on the cyclic displacement vs. number of cycles curve are shown in Fig. 3.

Histology

Following loading, bones were carefully removed from stainless-steel platens and fixed in 10% buffered formalin for 48 h. Bones were then bulk-stained for microscopic tissue damage using 1% basic fuchsin dissolved in increasing concentrations of alcohol using a previously described protocol [23]. Bones were kept in 70% solution for 8 h under vacuum (100 kPa, with a change of solution after 4 h) and overnight on the shaker in the same concentration. These steps were repeated with 1% basic fuchsin in 80, 90, and 100% alcohol solutions. Specimens were then put in 1% basic fuchsin in 100% alcohol for 48 h (with a change of solution after 24 h). Following staining, bones were washed two times in 100% alcohol (5 min each), cleared in methyl salicylate, and embedded undecalcified in methylmethacrylate. Three coronal sections of 250 μ thick were cut from each specimen using a low-speed diamond saw (Isomet low-speed saw; Buehler, Lake Bluff, IL) and polished to 100 μ thick with sandpaper (600 grit, followed by 1200 grit). These sections were then cleaned in distilled water under sonication and mounted on a glass slide for microscopy. Glass slides were examined under both bright field and epifluorescence at ×100 by an observer blinded to the loading conditions. To confirm that utilizing only three sections from each specimen was sufficient, all of the sections from specimens loaded into the tertiary phase or to failure were examined histologically (six or seven sections per specimen).

Four types of damage were evaluated: microcracks, diffuse damage, trabecular microfractures, and macroscopic cracks. Microcracks (20–100 μm long) were defined

the difference between the average cyclic displacements in the two blocks exceeded a predefined threshold value (end criteria), cyclic loading was stopped. Two end criteria were used to capture specimens in the tertiary phase: a late-tertiary phase criterion (corresponding to a rate of change in cyclic displacement of 1.6 μ/cycle) and an early-tertiary phase criterion (1.0 μ/cycle). If these criteria were not met within 5 h of loading, the test was stopped and the specimen classified as being in the early secondary phase (rate of change in cyclic displacement <0.5 μ/cycle) or in the late secondary phase (rate of change in cyclic displacement >0.5 μ/cycle) based on inspection of the cyclic displacement vs. number of cycles curve (Fig. 3). An additional three experiments were stopped after 30 min of loading to characterize the early secondary phase (and confirmed

as linear cracks observed under epifluorescent illumination and confirmed by viewing a halo of basic fuchsin staining under bright field illumination [4]. Diffuse damage was a region of generalized basic fuchsin staining observed in both fluorescent and bright field imaging. Trabecular microfractures consisted of a crack with basic fuchsin halo that crossed >75% or more of the observed trabecular thickness (shorter cracks were characterized as microcracks). Linear cracks larger than 200 µm in length in the cortical shell were characterized as macroscopic cracks. To consider regional differences in damage generation, these four types of damage were evaluated in the epiphyseal region, metaphyseal cancellous bone, and metaphyseal cortical bone. Trabecular bone area fraction (B.Ar/T.Ar) in the metaphyseal region was determined through point counting using an eyepiece grid reticule.

Statistical Analysis

Statistical tests were performed using Minitab software (Minitab® 15.1.0.0; Minitab, State College, PA) and custom software written for use with Matlab (MATLAB R2007a; MathWorks, Natick, MA). The Kruskal–Wallis test was performed to test the significant difference among study groups, and Dunnett's test was performed for multiple comparisons. Within each group, correlations between the amount of microdamage and trabecular bone volume fraction were determined. Additionally, the relationships between the number of microfractures and measures of loading (percent change in cyclic displacement, rate of change of cyclic displacement, etc.) were determined using linear regression.

Results

Four specimens stopped at the 1.6 µ/cycle criterion, six stopped at the 1.0 µ/cycle criterion, and six reached the specified time limit (5 h) and were characterized as run-out specimens. Five of the run-out specimens were classified as being in the late secondary phase, and one was classified being in the early tertiary phase. Microscopic tissue damage was observed in three different locations within the vertebrae: the epiphyseal region, the metaphyseal cancellous bone, and the cortical shell (Fig. 4). The amount of microscopic tissue damage was not associated with animal body weight, and no differences in damage were observed among the three different tail bones included in the study.

Trabecular microfracture (Fig. 5) was the primary form of microdamage that was observed in metaphyseal cancellous bone. The number of microfractures varied depending upon where the specimen was on the creep–fatigue curve, with increasing amounts of microfractures in
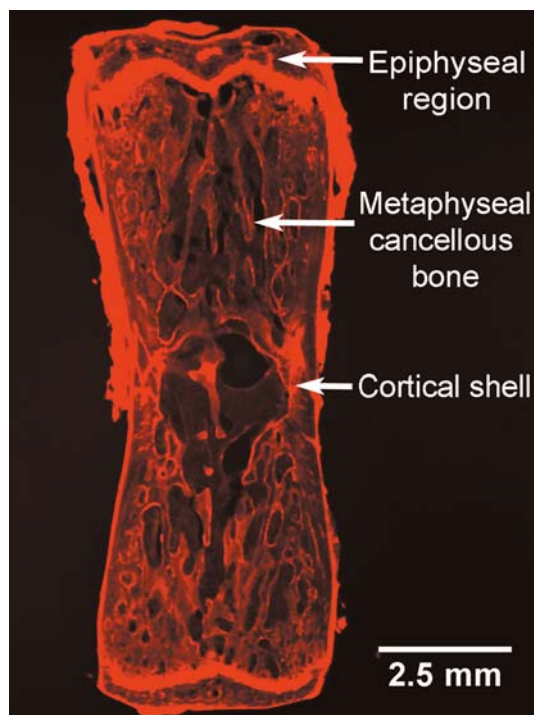

Fig. 4 Fluorescent image of a coronal section specifying the regions in which damage was classified
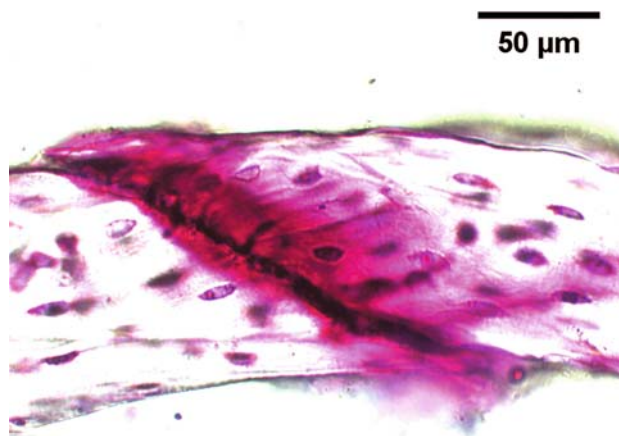
Fig. 5 A trabecular microfracture in a specimen loaded into the tertiary phase is shown

specimens stopped later in the creep–fatigue process (Fig. 6). Nine out of ten specimens loaded into the tertiary phase displayed at least one trabecular microfracture (Fig. 6). Bone volume fraction among specimens did not vary considerably (27.0 ± 4.8%, mean ± SD) and was not related to the number of microfractures. The percent change in cyclic displacement was correlated with the number of microfractures but was a poor predictor ($P = 0.04$, $r^2 = 0.23$). Few microcracks were observed in the metaphyseal cancellous bone (6 microcracks in 3 of the
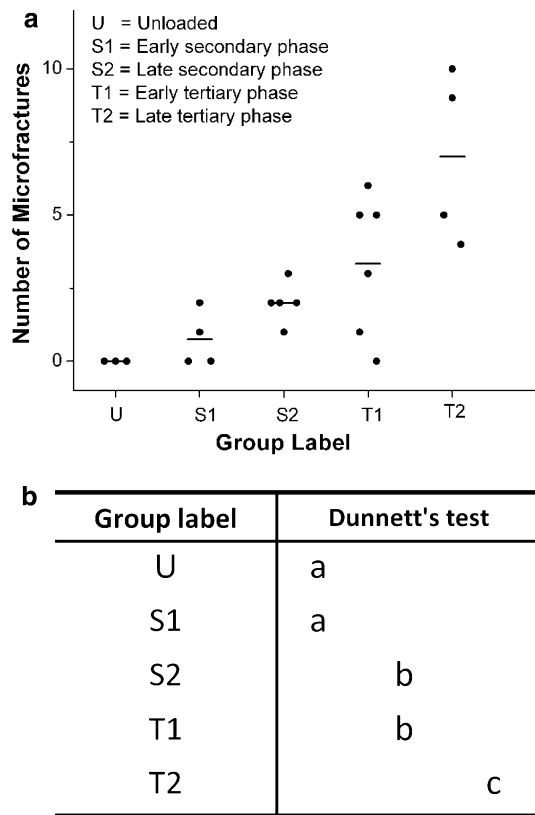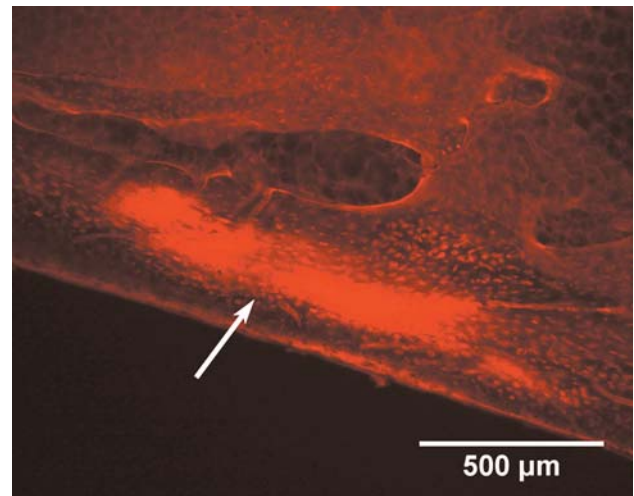
Fig. 6 a The number of microfractures observed in each test specimen is shown. *Horizontal lines* represent the group average. There was an increase in the number of microfractures in later phases of the creep–fatigue curve. b Results of Dunnett's multiple comparison test are shown. Group pairs with different letter combinations are significantly different from one another ($P < 0.05$). *U* unloaded, *S1* early secondary, *S2* late secondary, *T1* early tertiary, *T2* late tertiary

Fig. 7 Diffuse damage in the cortical shell (*arrow*)

Fig. 8 Macroscopic cracks in the cortical shell of failed specimens (*arrows*)

19 loaded specimens). No diffuse damage was observed in the metaphyseal cancellous bone.
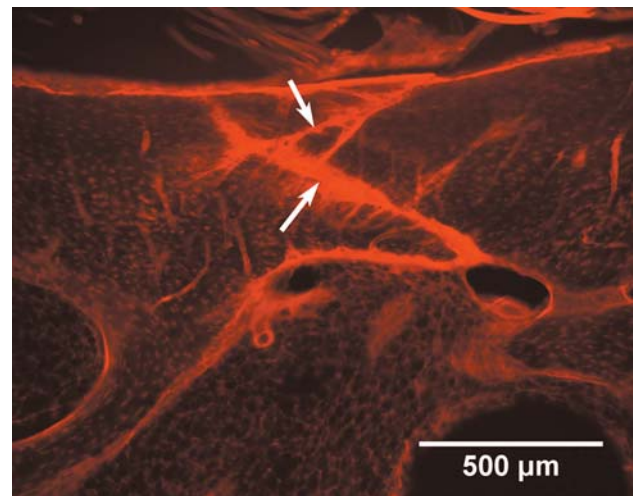
All loaded specimens displayed considerable diffuse damage in the epiphyseal cancellous bone. No trabecular microfractures or microcracks were observed in epiphyseal cancellous bone. Five out of ten specimens in the tertiary phase displayed small amounts of diffuse damage in the cortical shell (one patch of diffuse damage not >0.08 mm^2 per specimen, Fig. 7). No microcracks or macroscopic cracks were observed in the cortical shell of specimens stopped prior to failure. Specimens cyclically loaded to failure showed macroscopic cracks in the cortical shell (Fig. 8) along with diffuse damage. Additionally, specimens loaded to failure showed diffuse damage in the epiphysis and microfractures in the metaphyseal cancellous bone.

Discussion

The objective of the current study was to understand failure processes in rat caudal vertebra under axial cyclic loading.

Through in vitro testing we determined that cyclic axial overloading of the rat caudal vertebra causes microdamage in metaphyseal cancellous bone prior to failure or substantial microdamage in the cortical shell. Additionally, the amount of microscopic tissue damage in the metaphyseal cancellous bone was associated with the phase of the creep-fatigue loading curve. Trabecular microfracture was the primary form of microdamage observed in metaphyseal cancellous bone in the tail vertebrae. This finding suggests that axial overloading of rat tail vertebrae in vivo may be capable of generating microdamage to the cancellous bone without overt fracture or large amounts of microdamage to the surrounding cortical shell.

The current study had a number of strengths. First, the cyclic loading approach used a novel end criterion based on the rate of change of cyclic displacement. This end

criterion made it possible to stop each test after micro-damage had been generated but prior to complete failure. When using these end criteria we did not observe failure of the specimen. Another strength of the study is that bones were tested intact without removing the end plates. The presence of end plates has been shown to influence load distributions in vertebral trabecular bone [24], suggesting that loading applied with end plates intact may be necessary to mimic loading of cancellous bone in a live animal.

There are limitations that must be considered when interpreting our results, however. First, evaluation of microdamage was done on three mid-coronal, two-dimensional sections. It is possible that microdamage in trabecular bone or the cortical shell in other sections (sections close to the edges of vertebral body) may have been missed by this sectioning approach. However, our analysis of the specimens that experienced the greatest amount of cyclic overloading (the positive control and tertiary phase groups) included all coronal sections (six or seven sections per specimen). In the tertiary phase specimens (groups T1 and T2), no macroscopic cracks were observed and only small regions of diffuse damage were observed. Specimens loaded to failure displayed macroscopic cracks in the same coronal sections along with diffuse damage in the cortical shell, suggesting that our sectioning approach was able to detect microdamage in the cortical shell when present. Second, because bones were tested in vitro and potted in bone cement, the boundary conditions are expected to be different from what would be present in an in vivo loading situation. One of the main differences is that the system is more compliant in an in vivo scenario because of additional compliance from intervertebral discs and soft tissue around the vertebrae. For this reason, we expect the rat tail loading approach will need to be modified to achieve similar results in terms of microdamage in an in vivo loading situation. Lastly, the load magnitudes applied in the current study (0–260 N) are much greater than would be expected from normal physiological loading. The normal physiological activity (normal cage activity) of rats results in peak axial strain of approximately ± 140 $\mu\varepsilon$ in the cortical shell of the caudal vertebrae [25]. These kinds of strain correspond to axial loads <25 N on vertebra C8 (298 $\pm$ 105 $\mu\varepsilon$ at 25 N [26]). As a result, the failure modes we observed would not be expected to occur as a result of normal activity in the rat. In humans, however, trabecular microfracture is a well-recognized event [8–12], although it is not known what loading commonly results in trabecular microfracture.

Our approach for stopping the test before complete failure of a specimen was novel but most similar to the approach used by Uthgenannt and Silva [18] with the rat ulna loading model. Their end criterion was based on the percent displacement required for failure (as determined in preliminary studies). In our specimens, we found that the rate of change in cyclic displacement could more consistently stop the test prior to failure during cyclic overloading. An advantage of our end criterion is that, because it is based on the rate of change of displacement rather than total displacement, it is likely to be insensitive to small variations in bone size from animal to animal. Uthgenannt and Silva also observed trends between the amount of microdamage and the amount of applied loading but evaluated microdamage using micro-computed tomography rather than histology. It is unclear how microcracks observed using micro-computed tomography would be classified using histology (microcracks or macroscopic cracks). Waldorff et al. [21] applied loads to cancellous bone through a transcortical implant and observed trabecular microcracks but not trabecular microfractures. Differences in the form of microdamage between our study and the study by Waldorff et al. are most likely due to boundary conditions and the magnitude of applied loads. Waldorff et al. applied loads directly to the cancellous bone rather than through the cortical shell (as observed in the current study). Additionally, the animal model used by Waldorff et al. applied much smaller loads than used in the current study and did so in the transverse direction rather than the primary loading direction.

Our finding that trabecular microfracture is the primary form of microscopic tissue damage under this loading mode is not as surprising as it might first appear. A number of clinical studies have observed microscopic tissue damage (microcracks, trabecular microfracture) in human cancellous bone in the vertebrae as well as the femoral neck [8, 9]. The number of applied loading cycles in our study varied from approximately 5,000 (40 min of loading at 2 Hz) to 36,000 (5 h of loading at 2 Hz). These numbers of cycles suggest that our loading protocol would be characterized as "low cycle fatigue." In low cycle fatigue, failure is dominated by the propagation of a few larger cracks rather than accumulation of large amounts of small cracks. The failure processes observed in the current study in which microdamage was predominantly in the form of microfractures and not microcracks or diffuse damage is consistent with low cycle fatigue. That microscopic cracks were rarely observed suggests that, under these loading conditions, cracks, when formed, rapidly propagate to cause failure (trabecular microfracture in cancellous bone and overt failure in the cortical shell). It is possible that microcracks would be more common under testing at lower load amplitude for a longer time period (high cycle fatigue). However, the current study was limited to 5 h of loading based on advice from veterinary support regarding the maximum amount of time that might be appropriate to maintain an animal under anesthesia during in vivo loading.

There are currently two in vivo models for loading cancellous bone that do not require the use of a transcortical implant, the rat tail loading model [22, 26] and the axial tibial loading model [27, 28]. Although the current study evaluated loading in the rat tail vertebra, it suggests that it is possible to generate microscopic tissue damage in a whole bone without substantial damage to the surrounding cortical shell. As a result it may be possible to modify the rat tail loading model or the tibial axial loading model to study the formation and repair of microdamage. A challenge in adapting the rat tail loading model to this loading mode is that the current rat tail loading model applies loads through pins in the neighboring bones, and failure at high loads using that model tends to occur at the interface between the pins and the neighboring bones rather than the intermediary bone being loaded. A major limitation to generating microdamage in cancellous bone using the axial tibial loading model is the potential for painful damage to the knee joint, which could prevent the animal from continuing normal locomotion following the application of cyclic loading. While these are not trivial challenges, our observation that microdamage can be generated in cancellous bone without substantial damage in the surrounding cortical shell supports the idea that it is possible to study the generation and repair of microdamage in cancellous bone in an in vivo animal model.

References

1. Frost HM (1960) Presence of microscopic cracks in vivo in bone. Bull Henry Ford Hosp 8:27–35
2. Norman TL, Wang Z (1997) Microdamage of human cortical bone: incidence and morphology in long bones. Bone 20:375–379
3. Schaffler MB, Choi K, Milgrom C (1995) Aging and matrix microdamage accumulation in human compact bone. Bone 17:521–525
4. Burr DB, Stafford T (1990) Validity of the bulk-staining technique to separate artifactual from in vivo bone microdamage. Clin Orthop 260:305–308
5. Fazzalari NL, Forwood MR, Smith K, Manthey BA, Herreen P (1998) Assessment of cancellous bone quality in severe osteoarthrosis: bone mineral density, mechanics, and microdamage. Bone 22:381–388
6. Wenzel TE, Schaffler MB, Fyhrie DP (1996) In vivo trabecular microcracks in human vertebral bone. Bone 19:89–95
7. Vashishth D, Koontz J, Qiu SJ, Lundin-Cannon D, Yeni YN, Schaffler MB, Fyhrie DP (2000) In vivo diffuse damage in human vertebral trabecular bone. Bone 26:147–152
8. Todd RC, Freeman MA, Pirie CJ (1972) Isolated trabecular fatigue fractures in the femoral head. J Bone Joint Surg Br 54:723–728
9. Vernon RB, Pirie CJ (1973) Healing trabecular microfractures in the bodies of lumbar vertebrae. Ann Rheum Dis 32:406–412
10. Hernandez CJ, Tang SY, Baumbach BM, Hwu PB, Sakkee AN, van der Ham F, Degroot J, Bank RA, Keaveny TM (2005) Trabecular microfracture and the influence of pyridinium and non-enzymatic glycation-mediated collagen cross-links. Bone 37:825–832
11. Hahn M, Vogel M, Amling M, Ritzel H, Delling G (1995) Microcallus formations of the cancellous bone: a quantitative analysis of the human spine. J Bone Miner Res 10:1410–1416
12. Fazzalari NL (1993) Trabecular microfracture. Calcif Tissue Int 53(Suppl 1):S143–S147
13. Burr D (2003) Microdamage and bone strength. Osteoporos Int 14(Suppl 5):S67–S72
14. Burr DB, Forwood MR, Fyhrie DP, Martin RB, Schaffler MB, Turner CH (1997) Bone microdamage and skeletal fragility in osteoporotic and stress fractures. J Bone Miner Res 12:6–15
15. Kopperdahl DL, Pearlman JL, Keaveny TM (2000) Biomechanical consequences of an isolated overload on the human vertebral body. J Orthop Res 18:685–690
16. Torrance AG, Mosley JR, Suswillo RF, Lanyon LE (1994) Noninvasive loading of the rat ulna in vivo induces a strain-related modeling response uncomplicated by trauma or periosteal pressure. Calcif Tissue Int 54:241–247
17. Bentolila V, Boyce TM, Fyhrie DP, Drumb R, Skerry TM, Schaffler MB (1998) Intracortical remodeling in adult rat long bones after fatigue loading. Bone 23:275–281
18. Uthgenannt BA, Silva MJ (2007) Use of the rat forelimb compression model to create discrete levels of bone damage in vivo. J Biomech 40:317–324
19. Goldstein SA, Matthews LS, Kuhn JL, Hollister SJ (1991) Trabecular bone remodeling: an experimental model. J Biomech 24(Suppl 1):135–150
20. van der Meulen MC, Morgan TG, Yang X, Baldini TH, Myers ER, Wright TM, Bostrom MP (2006) Cancellous bone adaptation to in vivo loading in a rabbit model. Bone 38:871–877
21. Waldorff EI, Goldstein SA, McCreadie BR (2007) Age-dependent microdamage removal following mechanically induced microdamage in trabecular bone in vivo. Bone 40:425–432
22. Chambers TJ, Evans M, Gardner TN, Turner-Smith A, Chow JW (1993) Induction of bone formation in rat tail vertebrae by mechanical loading. Bone Miner 20:167–178
23. Burr DB, Hooser M (1995) Alterations to the en bloc basic fuchsin staining protocol for the demonstration of microdamage produced in vivo. Bone 17:431–433
24. Eswaran SK, Gupta A, Adams MF, Keaveny TM (2006) Cortical and trabecular load sharing in the human vertebral body. J Bone Miner Res 21:307–314
25. Kim CH, Takai E, Culella N, Guo XE (2002) Measurements of in vivo strains in the rat tail vertebra. In: Proceedings of ASME international mechanical engineering congress & exposition, IMECE 2002-32597
26. Guo XE, Eichler MJ, Takai E, Kim CH (2002) Quantification of a rat tail vertebra model for trabecular bone adaptation studies. J Biomech 35:363–368
27. De Souza RL, Matsuura M, Eckstein F, Rawlinson SC, Lanyon LE, Pitsillides AA (2005) Non-invasive axial loading of mouse tibiae increases cortical bone formation and modifies trabecular organization: a new model to study cortical and cancellous compartments in a single loaded element. Bone 37:810–818
28. Fritton JC, Myers ER, Wright TM, van der Meulen MC (2005) Loading induces site-specific increases in mineral content assessed by microcomputed tomography of the mouse tibia. Bone 36:1030–1038